

Article

# Processing Iron Oxide Nanoparticle-Loaded Composite Carbon Fiber and the Photosensitivity Characterization

Yong X. Gan <sup>1,\*</sup>, Christina Yu <sup>2</sup>, Niousha Panahi <sup>2</sup>, Jeremy B. Gan <sup>3</sup> and Wanli Cheng <sup>4,\*</sup>

<sup>1</sup> Department of Mechanical Engineering, California State Polytechnic University Pomona, Pomona, CA 91768, USA

<sup>2</sup> Department of Natural, Physical and Health Sciences, Citrus College, Glendora, CA 91741, USA; christinayu09@gmail.com (C.Y.); panahiniousha@gmail.com (N.P.)

<sup>3</sup> Diamond Bar High School, Diamond Bar, CA 91765, USA; jeremygan49@yahoo.com

<sup>4</sup> Troy High School, Fullerton, CA 92831, USA

\* Correspondence: yxgan@cpp.edu (Y.X.G.); 20009557@fjuhsd.org (W.C.); Tel.: +1-909-869-2388 (Y.X.G.)

Received: 18 February 2019; Accepted: 19 March 2019; Published: 22 March 2019



**Abstract:** In this work, iron oxide nanoparticle loaded carbon fibers were prepared by electrohydrodynamic co-casting a polymer and particle mixture followed by carbonization. The precursor used to generate carbon fibers was a linear molecular chain polymer: polyacrylonitrile (PAN). A solution containing iron (II, III) oxide ( $\text{Fe}_3\text{O}_4$ ) particles and the PAN polymer dissolved in dimethylformamide (DMF) was electrohydrodynamically co-cast into fibers. The fibers were stabilized in air and carbonized in hydrogen at elevated temperatures. The microstructure and composition of the fibers were analyzed using scanning electron microscopy (SEM). A quantitative metallographic analysis method was used to determine the fiber size. It was found that the iron (II, III) oxide particles distributed uniformly within the carbonized fibers. Photosensitivity of the particle containing fibers was characterized through measuring the open circuit potential of the fiber samples under the visible light illumination. Potential applications of the fibers for photovoltaics and photonic sensing were discussed.

**Keywords:** electrohydrodynamic co-casting; composite fiber; iron oxide nanoparticles; carbon fiber; photovoltaics; photonic sensor

## 1. Introduction

Iron oxide has been considered as a low-cost material with high energy storage capacity. Zhu et al. [1] made iron oxide/porous carbon nanofibers by electrospinning polyvinylpyrrolidone (PVP) and iron acetate and heat treating at 500 °C in nitrogen. The prepared porous nanofibers contain a carbon content of 12.5 wt.%. The iron oxide particles were coated with the carbon derived from PVP. The lithium ion battery anode made from the fibers showed improved cycling performance and rate capability. There are many other researchers who reported their work on this application [2–7]. For example, in the work performed by Xu et al. [4], iron oxide/carbon nanofibers ( $\text{FeO}_x/\text{CNFs}$ ) were prepared by electrospinning the  $\text{FeCl}_3 \cdot 6\text{H}_2\text{O}$ -polyacrylonitrile (PAN) precursors and heat treating at different temperatures. The iron oxide particles were embedded into the carbon nanofibers and used as the anodic electrode for rechargeable batteries. It was found that the oxidation states of iron in  $\text{FeO}_x/\text{CNFs}$  changed from  $\text{Fe}_2\text{O}_3$  to  $\text{FeO}$  and  $\text{Fe}$  with an improvement of capacity retention and an extra reversible capacity catalyzed by  $\text{Fe}$ .

In order to make high performance composite materials for supercapacitors, a solution containing polyacrylonitrile (PAN), polymethylmethacrylate (PMMA), and iron acetylacetonate ( $\text{FeAcAc}$ ) was

spun and followed by carbonizing the PAN [8]. The PMMA was pyrolyzed to form pores. Iron oxide nanoparticles were generated from FeAcAc. The elements Fe and O distributed throughout the carbon nanofibers. The pore formation due to the removal of the PMMA in the high temperature annealing process significantly shortens the diffusion path for ion transport at the electrode/electrolyte surface, which is considered as the reason for the high retention rate and high current density of the iron oxide/carbon fibers.

Carbon nanofibers decorated with iron oxide are also very effective in the removal of pollution contaminants from water [9–14]. The embedded iron oxide nanoparticles or iron-transition metal binary oxides play the important roles as poisoning metal sorbents. The heavy metals such as mercury and chromium can be effectively removed by the iron oxide/carbon fibers. Yang et al. [9] demonstrated the removal of  $\text{Hg}^0$  from coal combustion flue gas by the magnetic iron-manganese binary oxide supported on carbon nanofiber ( $\text{Fe}_{3-x}\text{Mn}_x\text{O}_4/\text{CNF}$ ). Iron oxide containing nanofibers are capable of removing arsenic compounds from water [12]. The fibers can be incorporated into filtration devices for metal oxyanions (arsenic- and chromium-containing compounds) removal [12]. In addition to eliminating poisoning metals from water, other compounds such as phosphate [13] and phenol [14] can be cleaned or removed from water by iron oxide modified oxides embedded into activated carbon fibers.

There are also reports on using iron oxide loaded carbon nanofibers for bio-sensing applications [15,16]. Porous carbon fibers with iron nanoparticles were used as the support for the Pt catalyst in direct methanol fuel cells [17]. It has been shown that some super-active sites can be introduced into carbon fibers with iron or nickel additives to achieve the high electrocatalytic performance [14,18]. Oxide-containing carbon fibers have demonstrated the potential for the photocatalytic application [19]. An electrostatic attraction approach using a green and facile solution was used to decorate carbon fibers with nanoparticles. The enhanced magnetic property was found in elastomer matrix composite materials containing the iron oxide decorated carbon fibers [20].

Although previous studies confirmed the promising applications of iron oxide nanoparticles/carbon fibers in energy storage, environment protection, and various other fields, there is little work on the photonic sensing and photovoltaic usages. It is the objective of this work to understand the photosensitive behaviour of the iron oxide/carbon composite fibers. We have used an electrohydrodynamic co-casting approach to prepare the precursor fibers (PAN-based fibers) first. Iron (II, III) oxide nanoparticles were embedded into the PAN fiber during the co-casting process. Then, a high temperature heat treatment procedure was carried out by converting the PAN fibers into partially carbonized fibers. To prevent the fully oxidation of the  $\text{Fe}_3\text{O}_4$  iron oxide and the burning of carbon fibers, hydrogen gas was used to generate a protective atmosphere during the high temperature heat treatment. Finally, the photosensitivity of the iron oxide-containing carbon fibers was characterized.

## 2. Materials and Methods

### 2.1. Materials and Instruments

A reusable stainless-steel dispensing needle with the gauge size of 20 (inside diameter of 0.6 mm), purchased from McMaster Carr Inc. (Santa Fe Spring, CA, USA), was used as the nozzle for the electrohydrodynamic casting of the polyacrylonitrile (PAN) polymer solution into fibers. The PAN polymer was procured from the company named Scientific Polymer Products, Inc. (Ontario, NY, USA). Its average molecular weight is about 150,000. The organic compound dimethylformamide (DMF) as a polar solvent, was purchased from Alfa Aesar (Ward Hills, MA, USA). It was used for the dissolution of the PAN polymer to form a uniform solution. The  $\text{Fe}_3\text{O}_4$  nanoparticles used in this study with a nominal diameter of 500 nm were purchased online from the chemical provider: Alpha Chemicals (Cape Girardeau, MO, USA). A direct current power supply with the highest output voltage of 30 kV was brought from Spellman High Voltage Electronics Corporation (Hauppauge, NY, USA). The Fusion

200 modular syringe pump used for polymer injection was purchased from Chemyx, Inc. (Stafford, TX, USA). A GSL-1100X tube furnace brought from MTI Corp (Richmond, CA, USA) was used for the two-stage high temperature treatment on the processed PAN fibers. In the initial stage of the treatment at 275 °C, PAN was oxidized and/or stabilized. The continued stage of treatment at 500 °C converted the PAN polymer fibers into partially carbonized fibers.

## 2.2. Electrohydrodynamic (EHD) Co-Casting

To prepare the PAN polymer solution for electrohydrodynamic (EHD) co-casting, 0.5 g of polymer powder was weighed by the use of a Model 311 OHAUS scale and about 5.0 mL of solvent, DMF, was fetched from the glassy storage bottle using a 10 mL plastic syringe. The 5.0 mL DMF was injected into a small beaker. Then, the PAN powder was added to the DMF to form a mixture with an approximate 10 wt.% content of PAN. The mixture was put into an ultrasonic machine to assist the dissolution of the PAN powder into DMF. To obtain a uniform solution of PAN in the DMF solvent, the beaker was set on a heating platform and kept at 45–50 °C for about half an hour. In addition, 0.05 g of iron (II, III) oxide was added into the solution. After that, the solution was poured into a PVC syringe. This syringe attached to a gauge 20 blunt metallic needle was placed into the rack of the precision pump. The electrohydrodynamic (EHD) co-casting was conducted under the fluidic pressure delivered by the precision pump and the static charge force due to the imposed high direct current (DC) potential at the tip of the needle. The pump injection rate was kept at 0.02 mL/min. The DC potential applied at the needle tip was 15 kV. The composite fibers came out from the needle and were co-cast onto a soft tissue paper. This paper was attached to a grounded aluminium plate. Once the EHD co-casting was done, the collected fibers were cut into samples for the subsequent processing. The oxidation of the PAN fiber and stabilization of its structure were carried out via heat treatment at 275 °C in air for 2 h. After that, the carbonization treatment was conducted at 500 °C in hydrogen atmosphere for 2 h. Figure 1 is the plot showing the time-temperature profile during the multiple stage high temperature treatment.

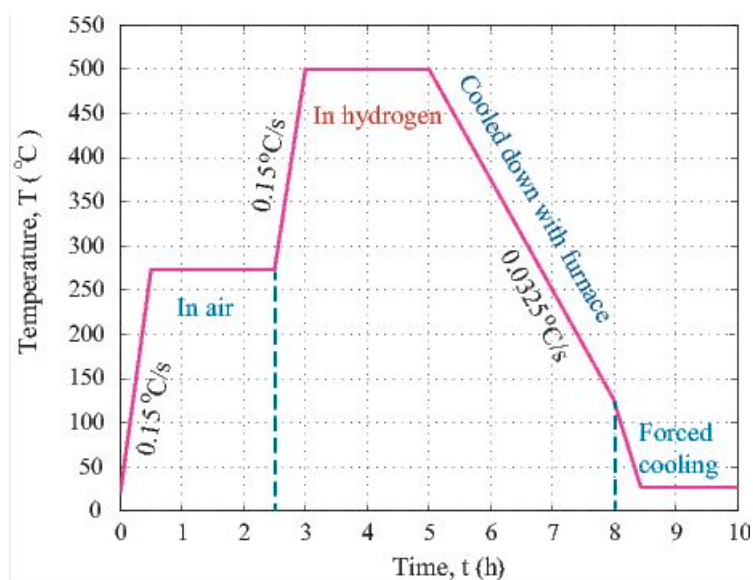


**Figure 1.** Temperature vs. time profile for heat treating the particle loaded fibers.

## 2.3. Microstructure Analysis

A JEOL JSM-6010PLUS/LA scanning electron microscope (SEM) (San Jose, CA, USA) was employed to examine the morphological features of the composite fiber. This SEM has an energy dispersive X-ray diffraction spectroscopy attachment. Analysis of elements in the fiber was done on the SEM via energy dispersive X-ray diffraction spectroscopy (EDS). A model 440C electrochemical

workstation, purchased from CH Instruments, Inc. (Austin, TX, USA), was employed for measuring the open circuit voltage or potential of the fiber when it was exposed to visible light illumination. The voltage vs. time data were obtained. The data were plotted to reveal the photosensitivity of the particle-containing fiber.

### 3. Results

This section is divided into two parts. The first part is on the morphological features and the chemical composition of the particle-containing fiber. The second part deals with the photosensitivity of the fiber under the visible light illumination.

#### 3.1. Structure of the Composite Fiber

The morphological features of the EHD co-cast composite fibers were revealed through the SEM by taking the secondary electron (SE) images. Both Figure 2a,b are the SEM images of the composite fibers after the oxidation heat treatment followed by carbonization in hydrogen reductive atmosphere. From the two images at different magnifications in Figure 2a,b, we can clearly see that the fibers are aligned in a fairly regular way. Iron oxide (II, III) nanoparticles are distributed uniformly within the fibers. In an image with a slightly higher magnification as illustrated by Figure 3a, the size of the fibers can be estimated around 0.83  $\mu\text{m}$ . The method for determining the fiber size was based on a quantitative metallographic analysis approach. We drew lines on the SEM micrograph and measured the length of the line segments overlapped by the fibers to determine their diameters. In a typical experiment, 103 samples were taken to measure the size of the fibers. It was found that the mean is 0.829  $\mu\text{m}$  and the standard deviation is 0.251  $\mu\text{m}$ . The results show that the standard deviation from the measurement is fairly high. This is due to the fact that some fibers are very fine (at nanoscale), while others are microfibers. Therefore, we simply called them fibers. The heat treatment in hydrogen gas changed the physical property of the fibers. We found that, before any heat treatment, the precursor PAN fibers are insulators. After the heat treatment, the PAN was partially carbonized. The composite fibers are semiconducting. Therefore, no sputter coating of conductive thin metal layer was used for the SEM observation.

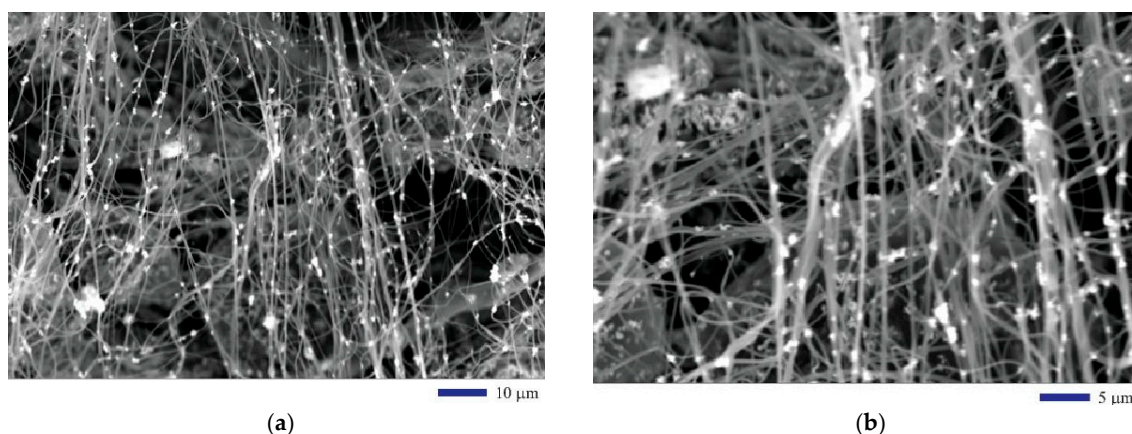


**Figure 2.** SEM images of the iron oxide nanoparticle-containing carbon fibers: (a) 1000 $\times$ ; (b) 2000 $\times$ .

The elements contained in the composite fiber were determined by the energy dispersive X-ray diffraction spectroscopy (EDS). In this study, the spot analysis of typical locations was carried out to reveal the composition information about each feature examined. Two locations with particular interest were chosen for the elemental analysis. One is at the fiber (Spot 001 as shown in Figure 3a; the other is at the particle as shown by Spot 002 in Figure 3a). The qualitative result based on the analysis of the fiber is shown in Figure 3b. Obviously, C, O, and N are the major elements found. It is evident that the  $K_{\alpha}$  peak of carbon is located at 0.28 keV. For oxygen, the  $K_{\alpha}$  peak is found at

0.53 keV. The quantitative results are shown in the first three data columns of Table 1. The analysis of the particle location, Spot 002, generated different result as revealed by Figure 3c. From Figure 3c, we can see that O, C, and Fe are the major elements generating high peaks. Besides the N and O characteristic peaks, more peaks belonging to the iron element can be observed. They are the  $K_{\alpha}$  peak of Fe found at 6.40 keV and  $K_{\beta}$  peak of Fe located near 7.06 keV. It must be noted that the  $L_{\alpha 1}$  (0.71 keV),  $L_{\alpha 2}$  (0.60 keV), and  $L_{\beta 1}$  (0.79 keV) peaks for iron were also shown in Figure 3c. The quantitative results associated with the analysis at Spot 002 are shown in data columns 4 to 8 of Table 1. It is found that the atomic percentage of carbon (C) is still high. The oxygen (O) amount found at Spot 002 is slightly lower than that found in the carbon fiber at Spot 001. Cu peak is also shown, but it is considered from the impurity in iron (II, III) oxide. Na is the other impurity element.

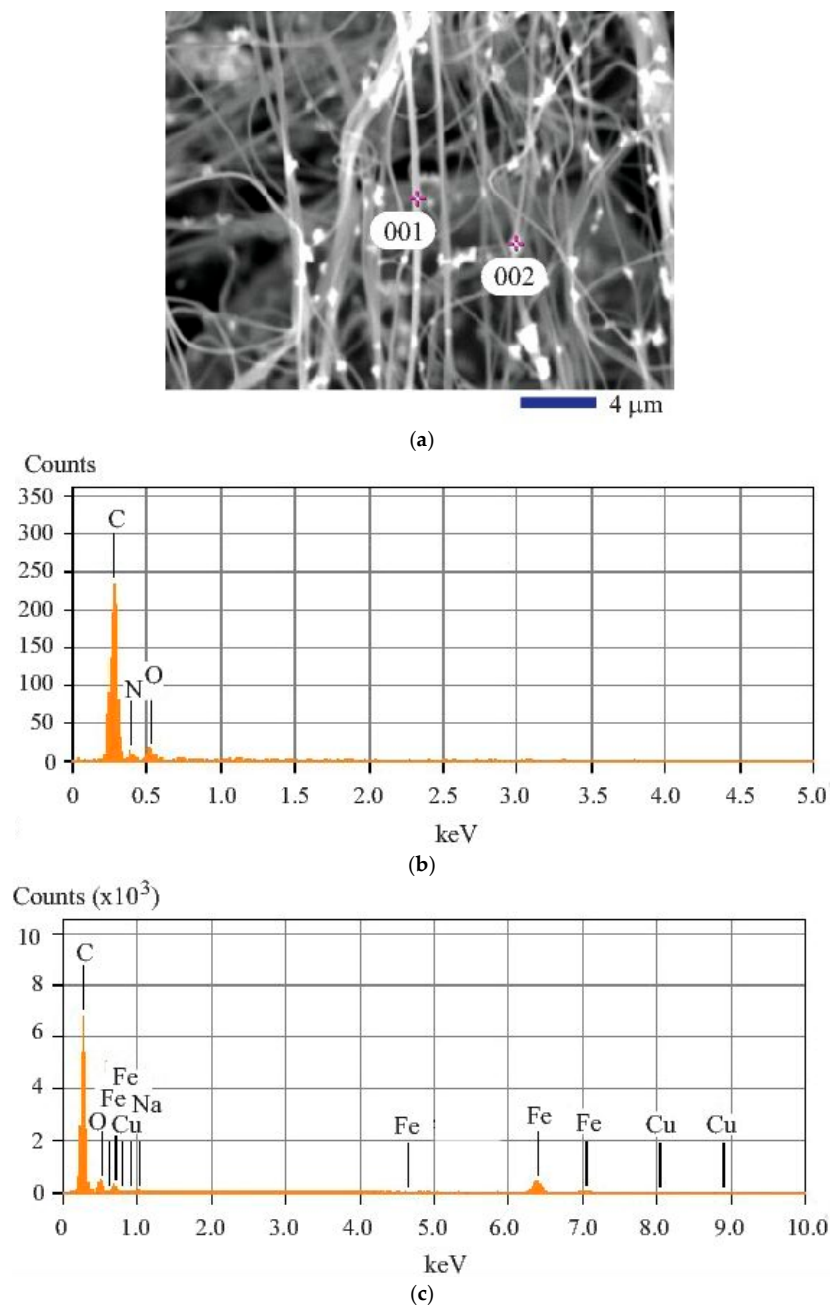


**Figure 3.** Image and composition analysis results of the iron (II, III) oxide nanoparticle-loaded carbon fibers: (a) SEM image at 3000 $\times$  showing the two spots for energy dispersive X-ray diffraction spectroscopy (EDS) analysis; (b) EDS obtained from Spot 001; (c) EDS obtained from Spot 002.

**Table 1.** Composition analysis results of the Fe<sub>3</sub>O<sub>4</sub>/carbon fiber (CF) specimen.

Location	Spot 001			Spot 002				
Element	C	O	N	C	O	Na	Fe	Cu
Atom %	86.79	10.54	2.67	86.32	9.13	0.16	4.15	0.24

It is worthy of investigating the structure evolution of the fiber during the multi-stage heat treatment. There are many early reports on the structure evolution of PAN from a linear molecular chain polymer to a cross linked one during high temperature treatment [21]. Basically, in the initial stage (Stage I) of the heat treatment, the oxygen from air caused the linear chains in PAN polymer cyclized. Such a cyclization allows the PAN polymer to transform into a ladder structured compound with better stability at elevated temperatures. In the temperature range from 200 °C to 300 °C, both cyclization and oxidation reactions in PAN happened [22]. In addition to the oxygen gas from air, some other inorganic oxidants, such as FeCl<sub>3</sub>, are also found effective to trigger the oxidation reaction in PAN even under room temperature conditions.

In the present study, we set the oxidation and stabilizing temperature at 275 °C. At this temperature, the colour of the polymer changed from white into yellowish brown. This is an indication that the linear structure of the PAN polymer was cyclized and converted into a non-meltable ladder structure as reported earlier in several other papers [23–25]. Since the absorbed oxygen entered into the PAN to form new functional groups, the initial stage of the treatment mainly caused the oxidation and stabilization of the polymer [26,27]. The second stage of the high temperature heat treatment (Stage II) at 500 °C is characterized by both condensation and carbonization. During this stage, most of the moieties or volatile impurities including NH<sub>3</sub>, H<sub>2</sub>O, HCN, and N<sub>2</sub> were released from the fiber. That is why the size of the fiber is reduced by 20% or more as shown early in [28].

### 3.2. Photosensitivity to Visible Light

To show the potential photonic applications of the iron oxide (II, III) nanoparticle-containing composite fiber, the photosensitivity and the photovoltaic behaviour of the fiber were characterized through recording the open circuit voltage of specimens under the visible light excitation. The time dependent open circuit voltage data were acquired by the use of the CH Instruments Inc. Model 440C electrochemical workstation. To establish the required conductive paths, two ends of the specimen were sandwiched by strips made of aluminium foil. These aluminium strips served as the electron collecting paths perfectly because of the high conductivity of aluminium. Three alligator jaw clips were used to clamp the ends of the specimen so that the connectivity with the reference electrode, counter electrode, and the working electrode can be built up.

Figure 4 reveals the photovoltaic response and photosensitivity of the composite fiber specimen consisting of the polymeric carbon fibers and the iron nanoparticles. In this figure, the open circuit potential vs. time data generated by the partially carbonized fiber loaded with iron nanoparticles under the illumination of a 120 W fluorescent light were plotted. The time-dependent potential data recording was initiated when the sample was covered by a light-blocking screen. After a while, the specimen was illuminated by the fluorescent light located 2 m away from the sample. The beginning cycle was 25 s; it was corresponding to the OFF state when the light source was blocked. Then, a following cycle with the ON state was coming, etc.

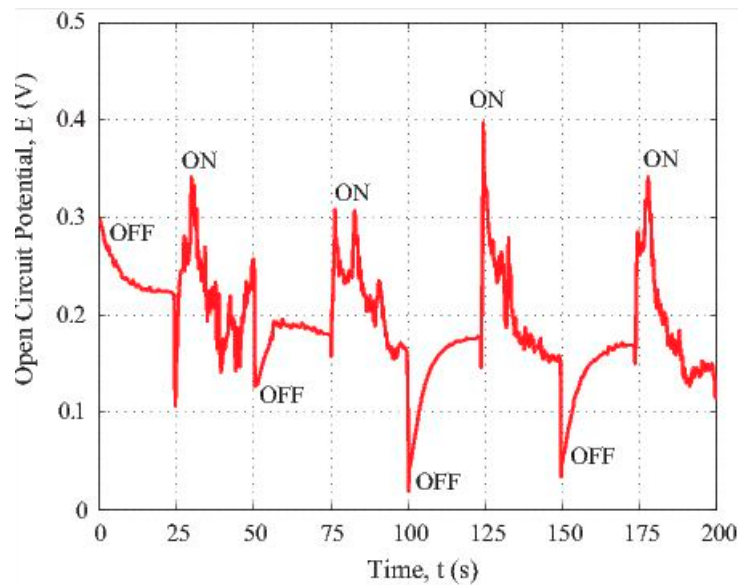


**Figure 4.** Photosensitivity of the iron oxide loaded carbon fiber under visible light excitation.

From the results illustrated in Figure 4, we can see that the difference between the maximum and minimum voltage values is about 0.4 V. The highest voltage was observed when the fluorescence light source was switched to the ON state. If the fluorescent light source was ON, the voltage was instantly generated by the specimen. The plot shows a jump of more than 0.2 V. Following this jump, the voltage drops gradually indicating the hole and the electron pair recombination. If we switched OFF the light, the potential suddenly dropped around 0.2 V. The positive voltage generation under ON state means that the carbon fiber loaded with iron nanoparticles showed an overall p-type behaviour. According to the report in [29], partially carbonized PAN polymer has a  $\pi$ -conjugated structure. There are localized electrons in such a structure. Chung [30] has proposed that there exists transition from n-type to p-type in semiconducting carbon fibres depending on the intercalation states within different carbon fibres.

To examine the transient state under visible light illumination, the open circuit potential data in the light ON cycle are plotted in Figure 5a. The decaying in the open circuit potential can be seen from Figure 5a. This comes from the relatively quick annihilation of electrons and holes due to the existence of the iron oxide nanoparticles. In order to determine the data trend, we developed a simple bi-exponential processing MATLAB code (The MATLAB used is the R2016a version released by The MathWorks, Inc., Natick, MA, USA). By using this code, the relevant parameters can be conveniently extracted by the computer. Figure 5b illustrates the general trend of the potential change with time,  $t$ , in the ON interval for the composite containing iron nanoparticles in the carbon fibers under the visible light illumination. We can adopt the following formula to fit the trend of the time-dependent open circuit potential,  $E$ , as used earlier in [31]:

$$E = Ae^{-mt} + Be^{-nt}, \quad (1)$$

where  $A$ ,  $B$ ,  $m$ , and  $n$  are materials parameters. It must be noted that  $m$  and  $n$  are the related time constants characteristic of the decaying in the open circuit voltage.

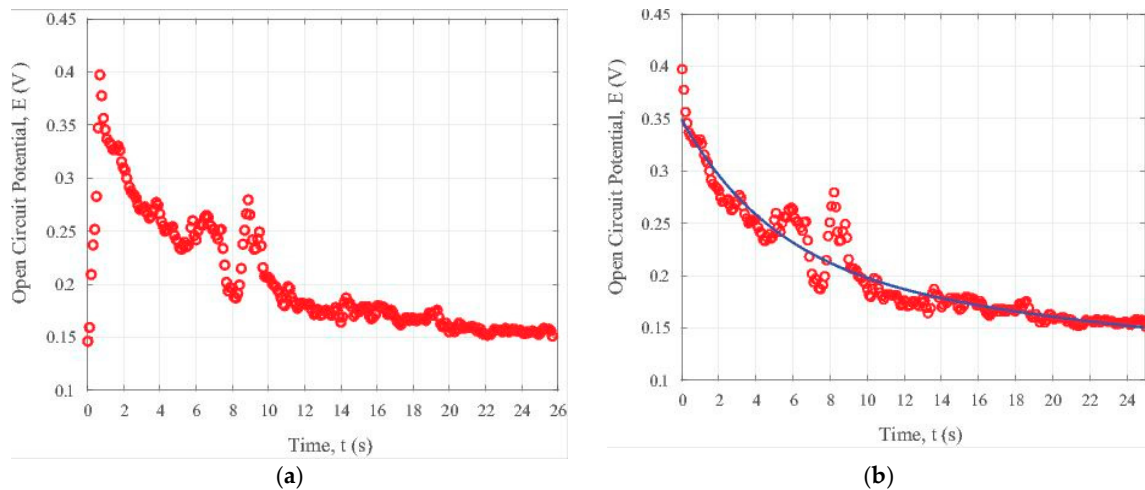


**Figure 5.** Transient photonic response of the iron oxide nanoparticle-loaded carbon fiber specimen under visible light illumination: (a) without data fitting, (b) with data fitting.

From the results shown in Figure 5b, it is possible for us to compute the four constants. The computation results show that  $A = -0.1606$  (V),  $B = 0.1884$  (V),  $m = 0.1885$ , and  $n = 0.0024$ . While the value for the time constant,  $\tau$  (with a unit of second), can be determined by:

$$\tau = n^{-1}. \quad (2)$$

Consequently, a bi-exponential data fitting gives:

$$E = -0.1606e^{-0.1885t} + 0.1884e^{-0.0024t}. \quad (3)$$

From the data fitting formula of Equation (3), the approximate value for the time constant  $\tau$  is 416.7 s. It is evident that both the formula as shown by Equation (3) and the data in Figure 5b reveal a slow decaying property, which is exactly required for some applications including photonic sensing, bio-imaging, and cell-labelling as discussed earlier in [31].

Similar bi-exponential data fitting was conducted for the light OFF testing cycle. The related constants were also extracted by the same MATLAB code, which yields:

$$E = -0.1528e^{-0.1941t} + 0.1965e^{-0.0111t}. \quad (4)$$

The time constant for the open circuit potential in the OFF cycle using the parameter in Equation (4) is about 90.09 s. Both the data sets and the fitted trend line were plotted and shown in Figure 6. It presents the trend of potential variation with the time elapsed for the iron oxide (II, III) nanoparticle loaded partially carbonized fiber specimen without visible light illumination. Comparing with the trend shown in Figure 5a for the specimen under visible illumination, we can see that Figure 6 clearly reveals a recovery behaviour when the light is OFF. Such a trend is due to the stable charge transport within the iron oxide containing carbon fibers. That is why the voltage decays in a stable way. On the contrary, the charge generation in the fibers is not so stable, as shown by the zig-zag shape of the curves in the ON state in Figure 4.

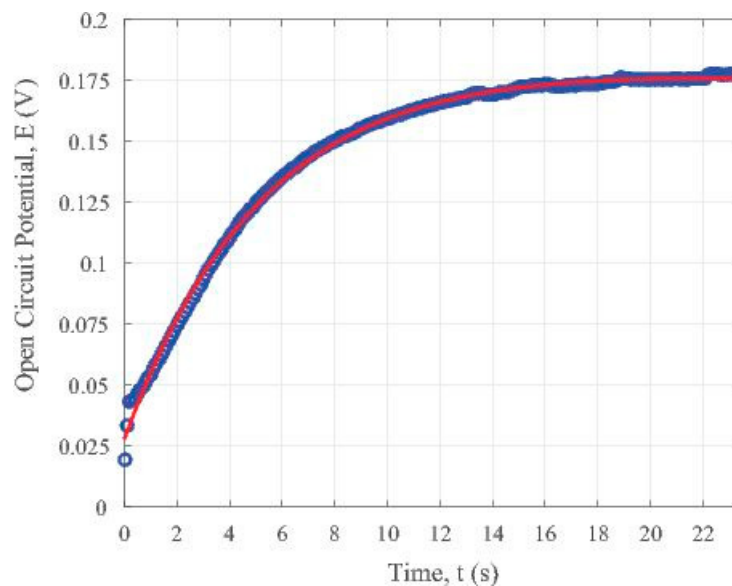


**Figure 6.** Recovery of the iron oxide nanoparticles loaded carbon fiber specimen after the shut off of the visible light illumination.

#### 4. Discussion

The method for determining the fiber size was purely based on the quantitative metallographic analysis method using the SEM micrographs. Such a preliminary measurement reveals that some of the fibers are as fine as nanoscale, while others are over 1 micron. Therefore, they are simply called fibers. The formation of such multiple scaled fibers depends on the processing conditions. The viscosity of the polymer solution is one of the significant parameters. Another factor is the existence of the iron oxide nanoparticles. The sites of the nanoparticles are the location with high charge density which causes the bifurcation of the polymer flow. Consequently, the fine strands of fibers at nanoscale come from the microfiber stems. It is also noted that the distribution of the nanoparticles in the fibers is fairly uniform only in a relative sense as compared with the cluster formation of oxide particles in the fibers extruded without applying the electric field. The imposed electric field helps remove the aggregation of nanoparticle clusters within the fibers. This is because the electrification of the particles generates repulsive forces between the adjacent particles. The repulsive forces push particles away from each other. The polymer flows allow the further separation of the adjacent particles.

Improving of the research has been considered focusing on the following aspects. First, there is an issue on the quality of the SEM images. For carbon fibers without iron oxide addition, the resolution of SEM image taken by the same JEOL JSM-6010PLUS/LA scanning electron microscope (SEM) is better. Once iron oxide particles were added, it was found that the conductivity of the composite fiber seems much lower than that of the carbon fiber. The charge of electron caused the blur of the image. Another reason for the blur of the image may be from the increased field depth due to the existence of the iron oxide particles in the fibers. To resolve this issue, the fibers may be coated with a conductive metallic layer, such as gold or palladium thin coating to reduce the charging tendency, and thus improve the image quality.

In view of the future research directions, we plan to study the effect of voltage level during the electrohydrodynamic co-casting on the distribution of the nanoparticles. The parameter effects, especially the heat treatment temperature on the conductivity of the composite fiber, will be investigated as well.

## 5. Conclusions

Iron oxide nanoparticle loaded carbon fibers have been successfully prepared by the single jet EHD co-casting approach. Such a method is suitable for generating long fibers. The iron (II, III) oxide nanoparticles are uniformly dispersed within the carbon fibers. It is believed that the electrification of the components in the mixture solution allows the uniform distribution of the iron oxide nanoparticles in the PAN fibers. Through the high temperature heat treatment in hydrogen, the partially carbonized composite fibers can be obtained.

Photosensitive and photovoltaic property studies of the iron oxide containing composite carbon fibers revealed the high sensitive to visible light. A general p-type semiconducting behaviour is confirmed. The composite fibers can generate electricity under the visible light illumination. The maximum absolute value of the potential obtained is over 0.4 V. The time constant of the polymeric carbon fibers is less than 0.2 s. The composite fibers have the potential to be used as the candidate materials for flexible solar panels and photonic sensors.

**Author Contributions:** Conceptualization, Y.X.G. and J.B.G.; methodology, Y.X.G. and C.Y.; software, Y.X.G.; validation, J.B.G., W.C., C.Y. and N.P.; formal analysis, Y.X.G.; investigation, W.C., J.B.G.; resources, Y.X.G.; data curation, C.Y. and N.P.; writing—original draft preparation, Y.X.G.; writing—review and editing, J.B.G. and W.C.; visualization, Y.X.G.; supervision, Y.X.G.; project administration, Y.X.G.; funding acquisition, Y.X.G.

**Funding:** This research was funded by National Science Foundation (NSF), Grant No. CMMI-1333044. The SEM images were made possible through the NSF Major Research Instrument (MRI) grant managed by Directorate of Materials Research (DMR) under Grant No. DMR-1429674.

**Acknowledgments:** C.Y. and N.P. were supported by the Citrus College Race to STEM Program co-managed by Marianne Smith at Citrus College and Winny Dong at California State Polytechnic University Pomona. Y.X.G. acknowledges the California State Polytechnic University Pomona 2017–2018 and 2018–2019 Provost's Teacher-Scholar support. We appreciate Anan Hamdan for his assistance in the SEM operation. Finally, we thank the two reviewers for providing constructive comments on improving the quality of the paper.

**Conflicts of Interest:** The authors declare no conflict of interest.

## References

1. Zhu, J.D.; Lu, Y.; Chen, C.; Ge, Y.; Jasper, S.; Leary, J.D.; Li, D.; Jiang, M.; Zhang, X. Porous one-dimensional carbon/iron oxide composite for rechargeable lithium-ion batteries with high and stable capacity. *J. Alloys Compd.* **2016**, *672*, 79–85. [[CrossRef](#)]
2. Guan, C.; Zhao, W.; Hu, Y.; Ke, Q.; Li, X.; Zhang, H.; Wang, J. High-performance flexible solid-state Ni/Fe battery consisting of metal oxides coated carbon cloth/carbon nanofiber electrodes. *Adv. Energy Mater.* **2016**, *6*, 1601034. [[CrossRef](#)]
3. Cho, J.S.; Park, J.S.; Kang, Y.C. Preparation of hollow Fe<sub>2</sub>O<sub>3</sub> nanorods and nanospheres by nanoscale Kirkendall diffusion, and their electrochemical properties for use in lithium-ion batteries. *Sci. Rep.* **2016**, *6*, 38933. [[CrossRef](#)]
4. Xu, Z.; Wang, L.; Wang, W.; Li, N.; Chen, C.; Li, C.; Yang, C.; Fu, H.; Kuang, L. Migration behavior, oxidation state of iron and graphitization of carbon nanofibers for enhanced electrochemical performance of composite anodes. *Electrochim. Acta* **2016**, *222*, 385–392. [[CrossRef](#)]
5. He, J.; Zhao, S.; Lian, Y.; Zhou, M.; Wang, L.; Ding, B.; Cui, S. Graphene-doped carbon/Fe<sub>3</sub>O<sub>4</sub> porous nanofibers with hierarchical band construction as high-performance anodes for lithium-ion batteries. *Electrochim. Acta* **2017**, *229*, 306–315. [[CrossRef](#)]
6. Xu, Z.L.; Yao, S.S.; Cui, J.; Zhou, L.M.; Kim, J.K. Atomic scale, amorphous FeO<sub>x</sub>/carbon nanofiber anodes for Li-ion and Na-ion batteries. *Energy Storage Mater.* **2017**, *8*, 10–19. [[CrossRef](#)]
7. Xu, X.; Wan, Y.; Liu, J.; Chen, Y.; Li, L.; Wang, X.; Xue, G.; Zhou, D. Encapsulating iron oxide@carbon in carbon nanofibers as stable electric conductive network for lithium-ion batteries. *Electrochim. Acta* **2017**, *246*, 766–775. [[CrossRef](#)]
8. Samuel, E.; Joshi, B.; Jo, H.S.; Kim, Y.; An, S.; Swihart, M.T.; Yun, J.M.; Kim, K.H.; Yoon, S.S. Carbon nanofibers decorated with FeO<sub>x</sub> nanoparticles as a flexible electrode material for symmetric supercapacitors. *Chem. Eng. J.* **2017**, *328*, 776–784. [[CrossRef](#)]

9. Yang, J.; Zhao, Y.; Liang, S.; Zhang, S.; Ma, S.; Li, H.; Zhang, J.; Zheng, C. Magnetic iron-manganese binary oxide supported on carbon nanofiber ( $\text{Fe}_{3-x}\text{Mn}_x\text{O}_4/\text{CNF}$ ) for efficient removal of  $\text{Hg}^0$  from coal combustion flue gas. *Chem. Eng. J.* **2018**, *334*, 216–224. [[CrossRef](#)]
10. Fard, G.C.; Mirjalili, M.; Almasian, A.; Najafi, F. PAMAM grafted alpha- $\text{Fe}_2\text{O}_3$  nanofiber: Preparation and dye removal ability from binary system. *J. Taiwan Inst. Chem. Eng.* **2017**, *80*, 156–167. [[CrossRef](#)]
11. Mohamed, A.; Osman, T.A.; Toprak, M.S.; Mohammed, M.; Uheida, A. Surface functionalized composite nanofibers for efficient removal of arsenic from aqueous solutions. *Chemosphere* **2017**, *180*, 108–116. [[CrossRef](#)] [[PubMed](#)]
12. Peter, K.T.; Johns, A.J.; Myung, N.V.; Cwiertny, D.M. Functionalized polymer-iron oxide hybrid nanofibers: Electrospun filtration devices for metal oxyanion removal. *Water Res.* **2017**, *117*, 207–217. [[CrossRef](#)] [[PubMed](#)]
13. Xiong, W.; Tong, J.; Yang, Z.; Zeng, G.; Zhou, Y.; Wang, D.; Song, P.; Xu, R.; Zhang, C.; Cheng, M. Adsorption of phosphate from aqueous solution using iron-zirconium modified activated carbon nanofiber: Performance and mechanism. *J. Colloid Interface Sci.* **2017**, *493*, 17–23. [[CrossRef](#)]
14. Han, C.; Jing, M.X.; Shen, X.Q.; Qiao, G.J. Electrospinning fabrication of mesoporous nano  $\text{Fe}_2\text{O}_3\text{-TiO}_2$ @activated carbon fiber membrane for hybrid removal of phenol from waste water. *Russian J. Appl. Chem.* **2016**, *89*, 2008–2015. [[CrossRef](#)]
15. Mondal, K.; Ali, M.A.; Singh, C.; Sumana, G.; Malhotra, B.D.; Sharma, A. Highly sensitive porous carbon and metal/carbon conducting nanofiber based enzymatic biosensors for triglyceride detection. *Sens. Actuators B Chem.* **2017**, *246*, 202–214. [[CrossRef](#)]
16. Fan, P.C.; Liu, L.J.; Guo, Q.H.; Wang, J.L.; Yang, J.H.; Guan, X.Y.; Chen, S.L.; Hou, H.Q. Three-dimensional N-doped carbon nanotube@carbon foam hybrid: An effective carrier of enzymes for glucose biosensors. *RSC Adv.* **2017**, *7*, 26574–26582. [[CrossRef](#)]
17. Shin, D.Y.; An, G.H.; Ahn, H.J. Iron-embedded porous carbon nanofibers as Pt electrocatalyst supports for direct methanol fuel cells. *J. Nanosci. Nanotech.* **2017**, *17*, 8180–8185. [[CrossRef](#)]
18. An, X.; Shin, D.; Jeong, J.; Lee, J. Metal-derived mesoporous structure of a carbon nanofiber electrocatalyst for improved oxygen evolution reaction in alkaline water electrolysis. *Chemelectrochem* **2016**, *3*, 1720–1724. [[CrossRef](#)]
19. Tissera, N.D.; Wijesena, R.N.; Sandaruwan, C.S.; Zhang, M.L.; Chen, Y.H.; Liu, Z.J.; Chen, H.S. Photocatalytic activity of ZnO nanoparticle encapsulated poly(acrylonitrile) nanofibers. *Mater. Chem. Phys.* **2018**, *204*, 95–206. [[CrossRef](#)]
20. Song, S.H. Synergistic effect of carbon nanofiber decorated with iron oxide in enhancing properties of styrene butadiene rubber nanocomposites. *J. Appl. Polym. Sci.* **2017**, *134*, 45376. [[CrossRef](#)]
21. Lee, S.; Kim, J.; Ku, B.C.; Kim, J.; Joh, H.I. Structural evolution of polyacrylonitrile fibers in stabilization and carbonization. *Adv. Chem. Eng. Sci.* **2012**, *2*, 275–282. [[CrossRef](#)]
22. Ma, Q.; Gao, A.; Tong, Y.; Zhang, Z. The densification mechanism of polyacrylonitrile carbon fibers during carbonization. *New Carbon Mater.* **2016**, *31*, 550–554. [[CrossRef](#)]
23. Hameed, N.; Sharp, J.; Nunna, S.; Creighton, C.; Magniez, K.; Jyotishkumar, P.; Salim, N.V.; Fox, B. Structural transformation of polyacrylonitrile fibers during stabilization and low temperature carbonization. *Polym. Degrad. Stab.* **2016**, *128*, 39–45. [[CrossRef](#)]
24. Liu, J.; Wang, P.H.; Li, R.Y. Continuous carbonization of polyacrylonitrile-based oxidized fibers: Aspects on mechanical properties and morphological structure. *J. Appl. Polym. Sci.* **1994**, *52*, 945–950. [[CrossRef](#)]
25. Wang, H.; Zhang, X.; Zhang, Y.; Cheng, N.; Yu, T.; Yang, Y.; Yang, G. Study of carbonization behavior of polyacrylonitrile/tin salt as anode material for lithium-ion batteries. *J. Appl. Polym. Sci.* **2016**, *133*, 43914. [[CrossRef](#)]
26. Sun, J.; Wu, G.; Wang, Q. The effects of carbonization temperature on the properties and structure of PAN-based activated carbon hollow fiber. *J. Appl. Polym. Sci.* **2005**, *97*, 2155–2160. [[CrossRef](#)]
27. Rahaman, M.S.A.; Ismail, A.F.; Mustafa, A. A review of heat treatment on polyacrylonitrile fiber. *Polym. Degrad. Stab.* **2007**, *92*, 1421–1432. [[CrossRef](#)]
28. Gan, Y.X.; Draper, C.W.; Gan, J.B. Carbon nanofiber network made by electrohydrodynamic casting immiscible fluids. *Mater. Today Commun.* **2017**, *13*, 248–254. [[CrossRef](#)]
29. Saha, B.; Schatz, G.C. Carbonization in polyacrylonitrile (PAN) based carbon fibers studied by ReaxFF molecular dynamics simulations. *J. Phys. Chem. B* **2012**, *116*, 4684–4692. [[CrossRef](#)]

30. Chung, D.D.L. Processing-structure-property relationships of continuous carbon fiber polymer-matrix composites. *Mater. Sci. Eng. Rep.* **2017**, *113*, 1–29. [[CrossRef](#)]
31. Gan, Y.X.; Panahi, N.; Yu, C.; Gan, J.B.; Cheng, W. Europium containing red light emitting fibers made by electrohydrodynamic casting. *Int. Nano Lett.* **2018**, *8*, 123–135. [[CrossRef](#)]



© 2019 by the authors. Licensee MDPI, Basel, Switzerland. This article is an open access article distributed under the terms and conditions of the Creative Commons Attribution (CC BY) license (<http://creativecommons.org/licenses/by/4.0/>).